

Article

The Ordovician Arc–Basin System in the Northern Great Xing’an Range (Northeast China): Constraints from Provenance Analysis of the Luohe Formation

Liyang Li ^{1,2}, Chuanheng Zhang ² and Zhiqiang Feng ^{3,*}

¹ Langfang Comprehensive Survey Center of Natural Resources, China Geology Survey, Langfang 065000, China; 18698263912@163.com

² School of Earth and Resources, China University of Geosciences, Beijing 100083, China; zhangch@cugb.edu.cn

³ Department of Earth Science and Engineering, Taiyuan University of Technology, Taiyuan 030024, China

* Correspondence: fengzhiqiang@tyut.edu.cn

Abstract: The Northeast China Block is a major component of the Central Asian Orogenic Belt, and its tectonic evolution has attracted much research attention. Ordovician strata are important in reconstructing the tectonic evolution of the Northeast China Block. This paper presents the results of sedimentological, zircon U–Pb, and geochemical analyses of sandstones of the Luohe Formation in the Wunuer area, Northern Great Xing’an Range, Northeast China. Lithological data, sedimentary structures, and grain-size analysis indicate that the Luohe Formation was deposited in a shallow marine environment. Detrital zircon U–Pb dating yields age peaks of 463, 504, 783, 826, 973, and 1882 Ma for sandstones from the Luohe Formation. The youngest zircon grain age of 451 ± 6 Ma represents the maximum depositional age of the Luohe Formation. The peak age at 463 Ma is consistent with the timing of post-collisional magmatism and the formation of the Duobaoshan island arc, while the peak at 504 Ma is consistent with the timing of magmatic activity related to the collision between the Erguna and Xing’an blocks. The peaks at 788, 826, 973, and 1882 Ma correspond to magmatism in the Erguna block, these ages indicate that the sandstones of the Luohe Formation were derived mainly from the Erguna block. Sandstone modal compositional analysis indicates that the provenance of the Luohe Formation was mainly a magmatic arc. The geochemical compositions of the sandstones suggest that the source rocks have continental island arc signatures. Based on the depositional age, sedimentary environment, provenance, and regional geology, it is concluded that the Luohe Formation was deposited in a back-arc basin setting during the formation of the Duobaoshan island arc–basin system in response to subduction of the Paleo-Asian oceanic plate.

Keywords: provenance analysis; tectonic setting; U/Pb spot ages; Northern Great Xing’an Range



Citation: Li, L.; Zhang, C.; Feng, Z. The Ordovician Arc–Basin System in the Northern Great Xing’an Range (Northeast China): Constraints from Provenance Analysis of the Luohe Formation. *Minerals* **2024**, *14*, 258. <https://doi.org/10.3390/min14030258>

Academic Editors: Yong Sik Gihm, Taejin Choi and Byung Choon Lee

Received: 8 February 2024

Revised: 22 February 2024

Accepted: 26 February 2024

Published: 29 February 2024



Copyright: © 2024 by the authors. Licensee MDPI, Basel, Switzerland. This article is an open access article distributed under the terms and conditions of the Creative Commons Attribution (CC BY) license (<https://creativecommons.org/licenses/by/4.0/>).

1. Introduction

The Central Asian Orogenic Belt (CAOB) is one of the largest and best-preserved Phanerozoic accretionary orogenic belts worldwide (Figure 1). It is located between the Siberian Craton–European Craton and the North China Craton–Tarim Craton, and, from west to east, it crosses the Ural Mountains through Kazakhstan, the Tien Shan, the Altai Mountains, and Mongolia to the eastern Pacific Ocean [1–11]. The CAOB records the tectonic evolution of the Paleo-Asian Ocean [8,12–15] and is one of the most prominent areas of continental crust growth globally, making it an ideal location in which to study accretionary orogenic processes and the growth of continental crust [4,8,16–19].

Northeast China is located in the eastern segment of the CAOB and comprises a collage of microcontinents, including (from southeast to northwest) the Songnen, Jiamusi, Xing’an, and Erguna blocks (Figure 2) [20–37]. The Erguna and Xing’an blocks were amalgamated into the Erguna–Xing’an block along the Xinlin–Xiguitu suture zone before

~500 Ma [20,27,30,38–43]; however, the mechanisms of subduction and collision between the Songnen and Erguna–Xing’an blocks remain unclear [29,37,41–47].

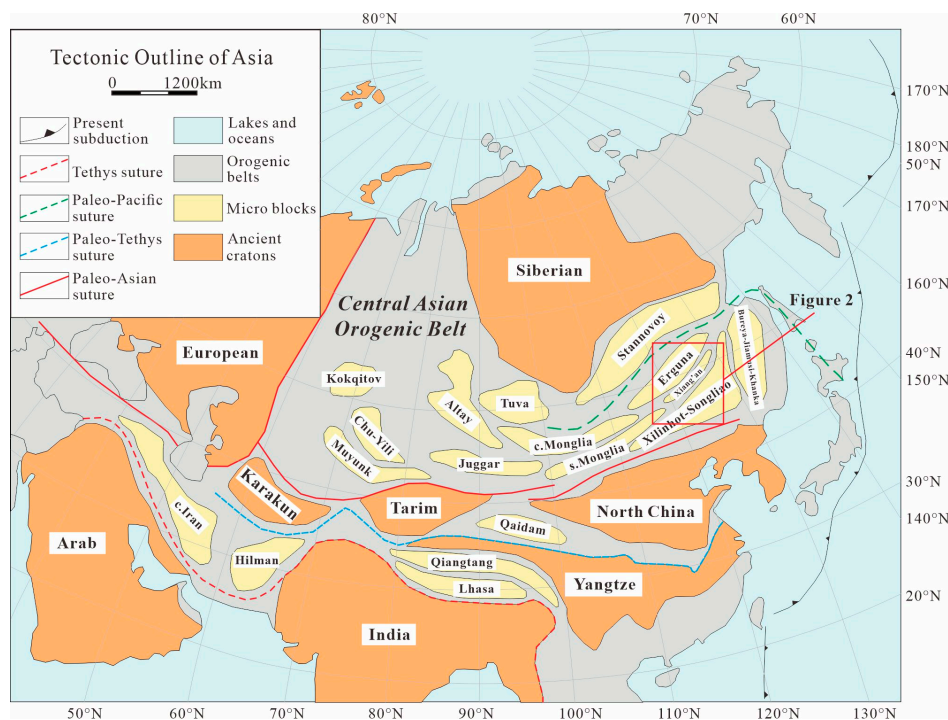


Figure 1. Tectonic sketch map showing the main tectonic domains of central and eastern Asia (modified from [28]).

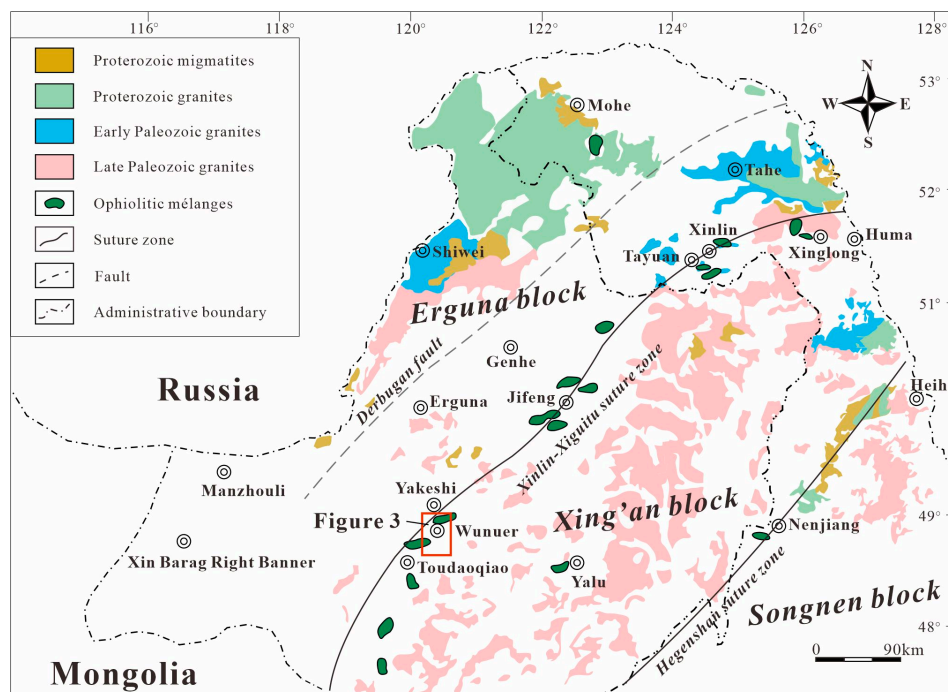


Figure 2. Tectonic division of the central-northern Great Xing’an Range (modified from [38,48]).

Previous studies on the tectonic evolution of the Erguna–Xing’an and Songnen blocks have focused mainly on magmatic rocks and ophiolites, with little attention paid to stratigraphy and sedimentology. Therefore, this study provides information on the depositional age, sedimentary environment, and provenance of the Ordovician Luohe Formation in

the Wunuer area, Northern Great Xing’an Range, Northeast China, to constrain the early Paleozoic tectonic evolution of the Erguna–Xing’an and Songnen blocks in Northeast China.

2. Geological Framework

2.1. Regional Geology

The study area is located between the Siberian and North China cratons and the Paleo-Pacific Plate, and it has been affected by the Paleo-Asian, Okhotsk, and Paleo-Pacific tectonic domains. During the Paleozoic era, the subduction and closure of the Paleo-Asian Ocean resulted in the formation of various Paleozoic sedimentary and magmatic rocks. The strata include the Ordovician Duobaoshan [39,49] and Luohe [50,51] formations and the Devonian Niquihe [52] and Daminshan [53] formations, with Silurian strata being absent. Paleozoic magmatic rocks include early Carboniferous diorite and granodiorite and late Carboniferous monzogranite and syenite [54,55]. Since the Mesozoic era, the study area has been influenced by the tectonic evolution of the Okhotsk and Paleo-Pacific oceanic domains. Mesozoic volcanic rocks are widespread in the study area and include the Manketouebo, Manitou, and Baiyingaolao formations [56,57] (Figure 3). The Luohe Formation is in fault contact with the Duobaoshan Formation, is unconformably overlain by Mesozoic volcanic rocks, and is intruded by Carboniferous and Ordovician magmatic rocks.

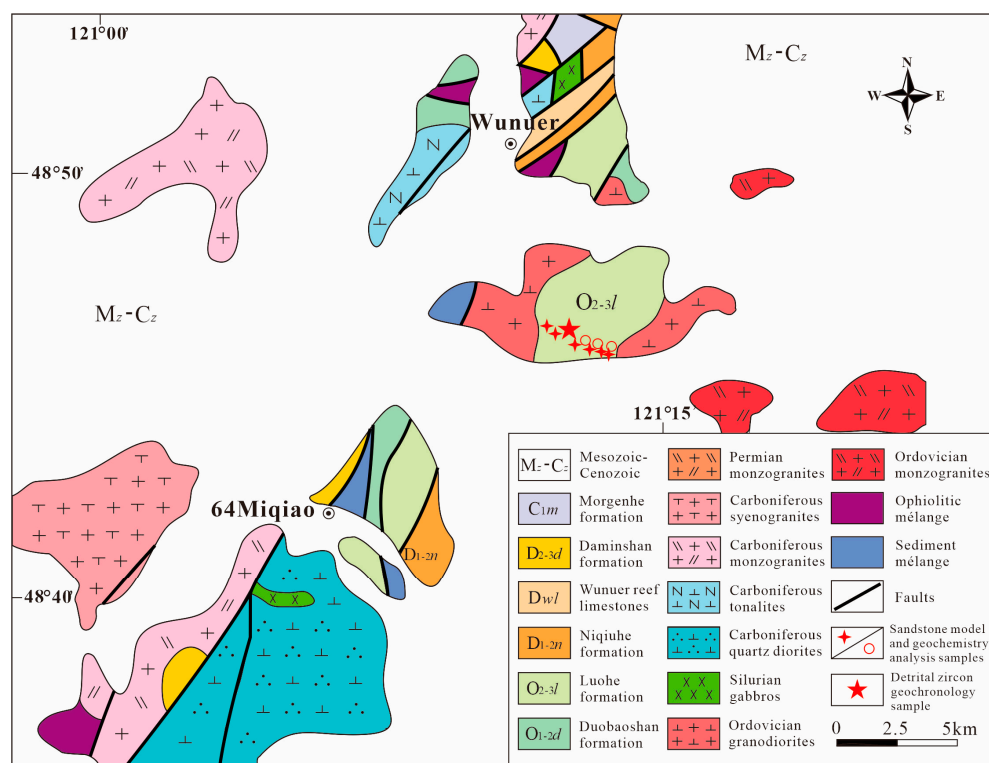


Figure 3. Geological map of Wunuer area with sample locations (simplified and modified after the 1:50,000 geological map).

2.2. Sampling

The studied section of the Luohe Formation has a thickness of 1435 m. The lower part of the formation is composed mainly of fine- to coarse-grained feldspathic litharenite, with graded and parallel bedding. The upper part of the formation is composed mainly of horizontally bedded siltstone and mudstone, with minor fine-grained feldspathic litharenite (Figure 4).

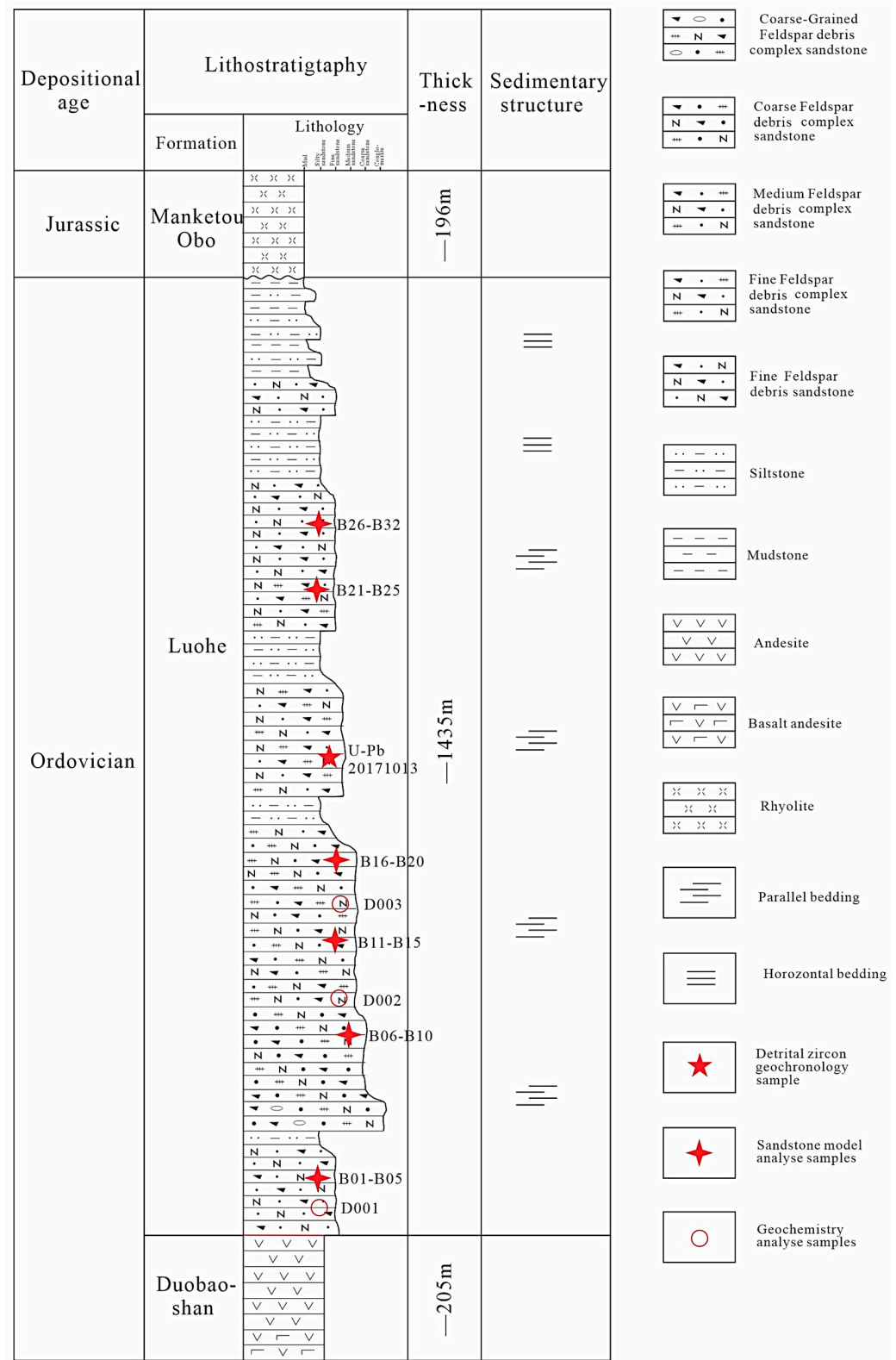


Figure 4. Schematic lithostratigraphic succession of the Luohe Formation showing sample locations.

One sample of fine- to medium-grained sandstone (sample 20171013) was collected from the middle part of the Luohe Formation for detrital zircon geochronology (Figures 3 and 5). The sandstone was a greyish-green color with parallel bedding and consisted of lithic fragments (35%, mainly volcanic), feldspar (30%), and quartz (35%).

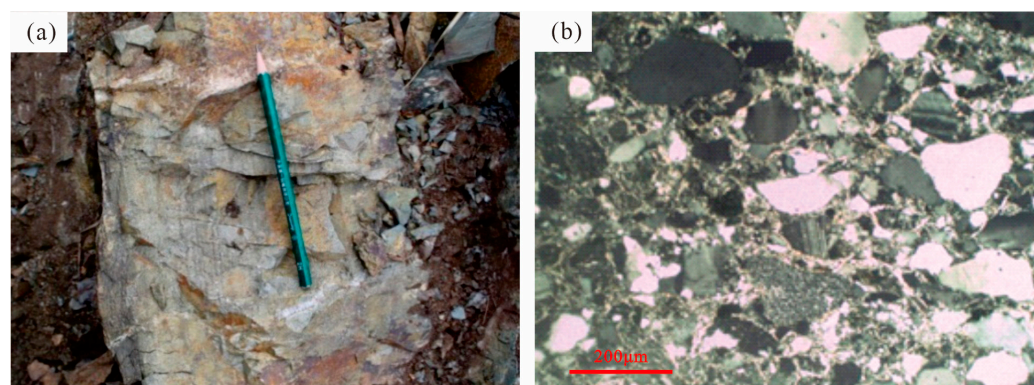


Figure 5. (a) Field photograph and (b) photomicrographs of sample 20171013.

We collected 32 hand samples of medium- to coarse-grained sandstone for analysis of the sandstone modal compositions (Figures 3 and 5). The samples were a greyish-green color with parallel bedding and consisted of lithic fragments (30%–35%, mainly volcanic), feldspar (30%–35%), and quartz (35%–40%).

Three samples of medium- to coarse-grained sandstone were collected from the middle and lower parts of the Luohe Formation for geochemical analysis (Figures 3 and 5). The samples were a greyish-green color with parallel bedding and consisted of lithic fragments (30%–35%, mainly volcanic), feldspar (30%–35%), and quartz (35%–40%).

We collected 33 samples for sedimentary grain-size analysis. The samples were evenly distributed throughout the Luohe Formation. Those from the lower and middle parts were mainly medium- to coarse-grained sandstones, and those from the upper part were mainly fine- to medium-grained sandstone with horizontal bedding.

3. Analytical Methods

3.1. Detrital Zircon Geochronology

Zircon separation and cathodoluminescence imaging were carried out at Beijing Geo-analysis Co. Ltd., Beijing, China. Zircon U–Pb isotope analyses were performed at Beijing Createch Testing Technology, Beijing, China. The analyses employed a SIUP193FXArF LA system and a ThermoFisher Neptune multi-receiver inductively coupled plasma–mass spectrometry (ICP–MS) instrument, with a laser spot diameter of 35 μm , laser energy of 10–13 J/cm^2 , and frequency of 8–10 Hz. Zircon U–Pb age data were calculated using Isoplot 3.00 software [58]. The standard zircon 91500 with an age of 1065.4 ± 0.6 Ma was used for calibration, the zircon 91500 consists of one crystal with an original mass of 238 g, which was provided by the Harvard Mineralogical Museum in Cambridge, USA. The original collection site of the zircon 91500 is recorded as Kuehl Lake in Ontario, Canada. The predominant rock type at this locality is porphyroblastic syenite gneiss which is cross-cut by sheets or sills of syenite pegmatite. This earlier characterization reported a near concordant U–Pb age of 1065 Ma for this crystal, and the 91500 zircon is widely used for in situ U–Pb zircon dating as a standard sample globally [59–61].

3.2. Sandstone Modal Analyses

Point counting of 32 thin sections of sandstone samples was undertaken using a polarizing microscope. For each thin section, >400 framework grains were counted and categorized according to a modified Gazzi–Dickinson method [62], in which crystals larger than silt within lithic grains were counted as monocrystalline grains. Matrix and cement were not counted, and grains within plutonic rock fragments were counted separately, so that the relative proportions of the plutonic rock fragments could be documented.

3.3. Geochemistry Analyses

Whole-rock geochemical analyses were performed at the Analytical Laboratory of the Beijing Research Institute of Uranium Geology, Beijing, China. Major element analyses were conducted on an AxiosmAX X-ray fluorescence spectrometer, and the analytical precision was ~5%. Trace element analyses employed a NexION300D ICP-MS instrument, and the analytical precision was better than 10%.

3.4. Sedimentary Grain Size Analysis

Grain-size analysis was conducted at the Hebei Provincial Institute of Regional Geological and Mineral Survey, Langfang, China. Thin sections were prepared for analysis under an Olympus BX53 polarizing microscope. Particle size and type were measured by visual estimation according to the Gazzi–Dickinson point-counting method, and then the particles were screened out and impurities corrected. A total of 600 grains of >0.004 mm in size were counted in each sample. The mean grain size (MZ), standard deviation (SD), skewness (SK), and kurtosis (KG) were calculated using the Method of Moments. All particle-size parameters were calculated using Fokker and Ward’s formula. Cumulative probability and frequency curves were drawn using Origin 8.0 software.

4. Results

4.1. Zircon U–Pb Geochronology

A total of 120 zircons were analyzed. The zircons are mainly short columnar crystals with widths of 50–100 μm , lengths of 100–150 μm , and fine-scale oscillatory zoning (Figure 6). The Th/U ratios of the zircons are 0.10–1.28, indicating a magmatic origin. Seven analyses were discarded owing to high discordance (Table S1). The remaining 113 analyses yield apparent ages of 451 ± 5.6 to 2765 ± 19 Ma and fall into four main age populations: (1) 451 ± 6 to 499 ± 6 Ma ($n = 24$) with a peak at 463 Ma; (2) 500 ± 5 to 559 ± 6 Ma ($n = 50$) with a peak at 504 Ma; (3) 707 ± 14 to 1004 ± 12 Ma ($n = 31$) with peaks at 783, 826, and 973 Ma; and (4) 1321 ± 24 to 2766 ± 20 Ma ($n = 8$) with a peak at 1882 Ma (Figure 7).

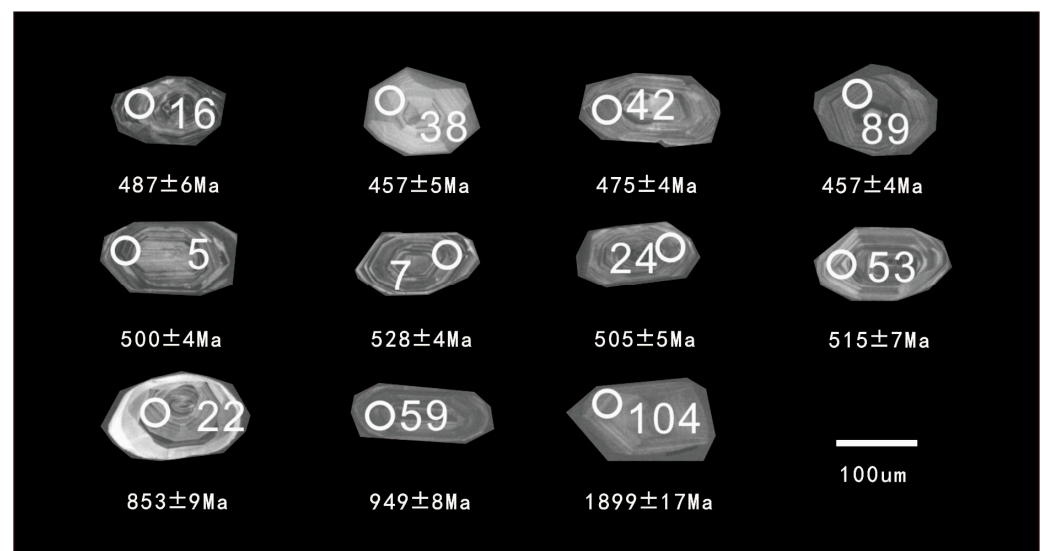


Figure 6. Cathodoluminescence (CL) images of detrital zircons from sample 20171013. The circles represent numbered U–Pb analysis sites, with ages presented below.

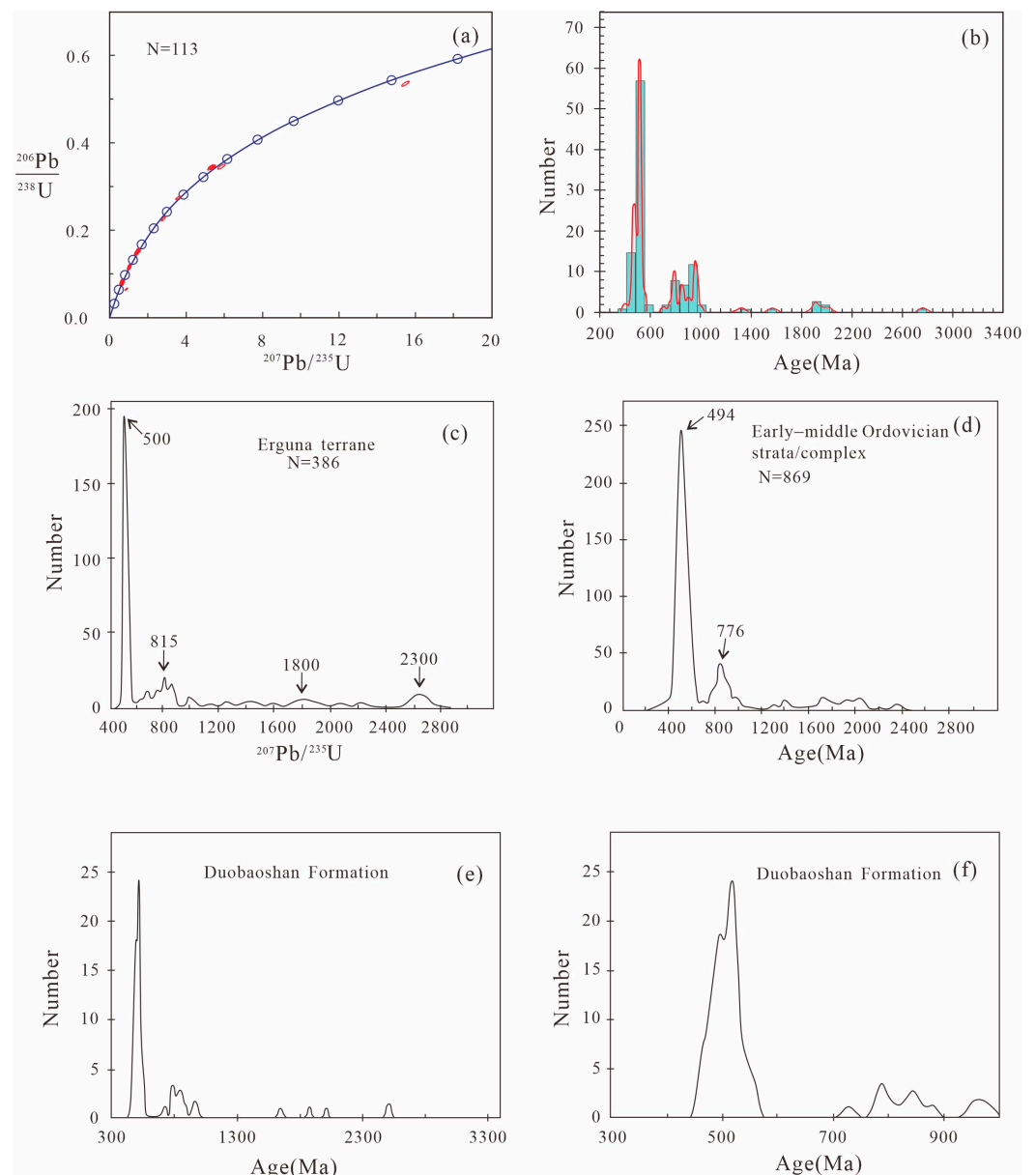


Figure 7. (a,b) Zircon U–Pb concordia and age probability diagrams for sample 20171013. (c) Age probability diagram for zircons from the Erguna terrane, from [63] (d) Age probability diagram for zircons from the Early–Middle Ordovician strata/complex, from [63]. (e,f) Age probability diagrams for zircons from the Duobaoshan Formation, from [64].

4.2. Sandstone Modal Analyses

The sandstone samples used for modal analysis are moderately cemented and moderately to poorly sorted with subangular to subrounded framework grains. The sandstones are medium- to coarse-grained sandstones (Figure 8). The results indicate that the samples comprise 20%–40% lithic fragments (mainly volcanic), 15%–35% feldspar grains, and 25%–45% quartz grains (mainly monocrystalline), and the ratio of monocrystalline quartz to polycrystalline quartz is 28:5, the ratio of volcanic-metavolcanic rock fragment to sedimentary-metasedimentary rock fragment is 28:3 (Table S2).

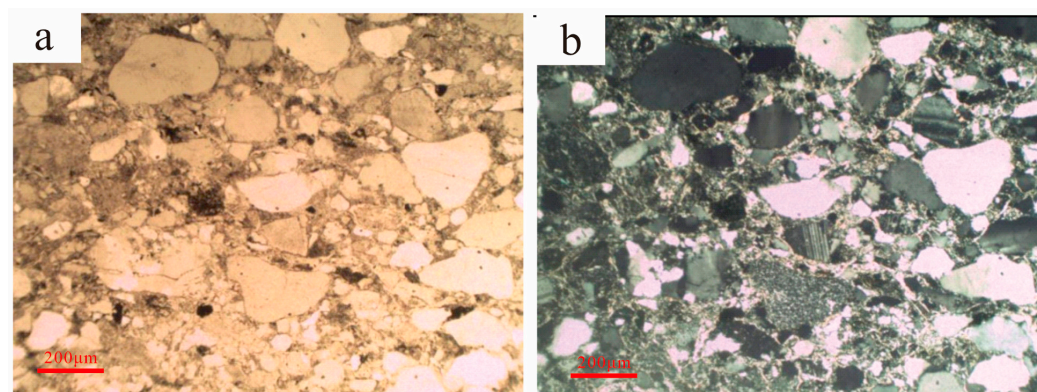


Figure 8. Representative photomicrographs used for sandstone modal analyses. (a) The photomicrographs under single polarizer and (b) the photomicrographs under crossed polarizer.

4.3. Geochemistry Analyses

4.3.1. Major Elements

The studied sandstones contain SiO_2 (58.79–61.25 wt.%), Al_2O_3 (17.19–18.43 wt.%), $\text{Na}_2\text{O} + \text{K}_2\text{O}$ (5.11–5.32 wt.%), TiO_2 (0.41–0.61 wt.%), MgO (3.83–4.17 wt.%), and $(\text{Fe}_2\text{O}_3)^T$ (7.33–7.64 wt.%), with $\text{N}_2\text{O}/\text{K}_2\text{O}$ values of 0.22–0.61. The samples are rich in Si, Al, and Fe, and poor in Mn, P, and Mg (Table 1).

Table 1. Major element data of sandstones from the Luohe Formation in the Wunuer area (wt.%).

Sample	Rock	SiO_2	Al_2O_3	Fe_2O_3	MgO	CaO	Na_2O	K_2O	MnO	TiO_2	P_2O_5	LOI	TOTAL
D001	Feldspar lithic sandstone	61.25	17.19	7.48	3.87	0.43	1.53	3.77	0.12	0.74	0.16	3.43	99.97
D002	Feldspar lithic sandstone	58.79	18.43	7.64	3.83	0.38	0.96	4.36	0.45	0.78	0.16	4.16	99.94
D003	Feldspar lithic sandstone	60.61	17.35	7.33	4.17	0.47	1.93	3.18	0.13	0.73	0.17	3.9	99.97

4.3.2. Trace Elements and REE

The sandstones are relatively enriched in Rb and U, and depleted in Nb, Sr, P, and Ti. Their chondrite-normalized rare earth element (REE) patterns exhibit uniform distributions and are characterized by moderate enrichment in light REEs (LREEs) and relatively flat heavy REEs (HREEs). In addition, the sandstones exhibit slightly negative Eu anomalies (Table 2; Figure 9a,b).

Table 2. Trace element data of sandstones from the Luohe Formation in the Wunuer area (ppm).

Sample	Rock	Rb	Ba	Th	U	Nb	La	Ce	Sr	Nd	Zr	Hf	Sm
D001	Feldspar lithic sandstone	276	410	10.9	2.71	12.4	29.6	62.4	81.7	29	59.2	2.09	5.76
D002	Feldspar lithic sandstone	424	426	10.2	3.73	11.8	45.7	60.5	210	38.4	69.3	2.06	7.75
D003	Feldspar lithic sandstone	235	370	10.3	2.26	11.4	23.6	48.9	85.3	24.3	52.8	1.88	5.1
Sample	Rock	Pr	Eu	Gd	Tb	Dy	Ho	Er	Tm	Y	Yb	Lu	
D001	Feldspar lithic sandstone	7.37	1.07	5.38	0.72	3.67	0.721	2.14	0.304	22	2.01	0.306	
D002	Feldspar lithic sandstone	10.6	0.995	6.9	0.944	4.9	0.959	2.92	0.419	29.1	2.86	0.433	
D003	Feldspar lithic sandstone	6	0.999	4.74	0.646	3.39	0.675	2.02	0.285	20	1.89	0.285	

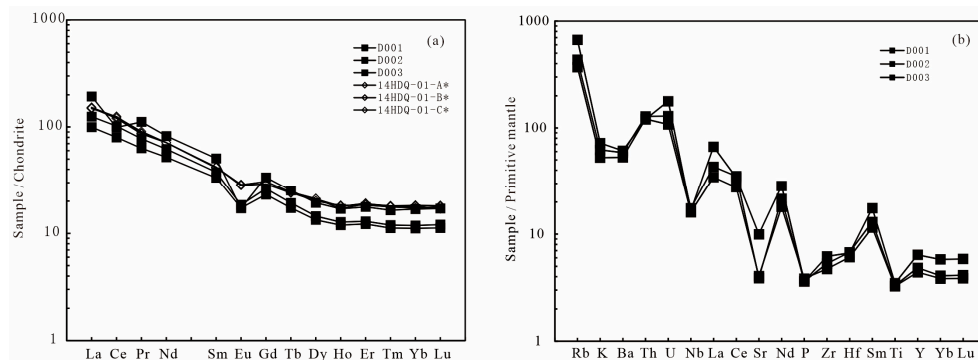


Figure 9. (a) Chondrite-normalized REE patterns and (b) primitive-mantle-normalized trace element spidergrams for samples from the Luohe Formation (\square from this study; \diamond from [64]).

4.4. Sedimentary Grain-Size Analysis

The grain-size characteristics of sedimentary rocks are influenced by transport and depositional processes and can be used to infer the sedimentary environment [65]. The grain size of the studied samples is mainly $\sim 2\phi$ (where ϕ is the average particle size), and grain-sizes fall in a range of 1ϕ – 4ϕ , indicating that the samples are mainly fine–medium sandstone. Standard deviation values are 0.5–0.8; therefore, the samples are moderately sorted to moderately well sorted (Table S3). Cumulative probability curves for the samples display a three-stage distribution (Figure 10), representing three phases of sediment movement; i.e., jump, shift, and suspension. The first stage is between 75% and 90%, representing the jump formation. The second stage is between 5% and 15%, representing the movement formation. The third stage is between 5% and 10%, representing the suspension formation. The grain-size frequency curves are characterized by a single peak and exhibit nearly symmetrical negative skewness and sharp or very sharp distributions. According to grain-size discriminant analysis [66], the calculated Y values for the studied samples are all >65 . The above features indicate that the Luohe Formation was deposited in a shallow marine setting.

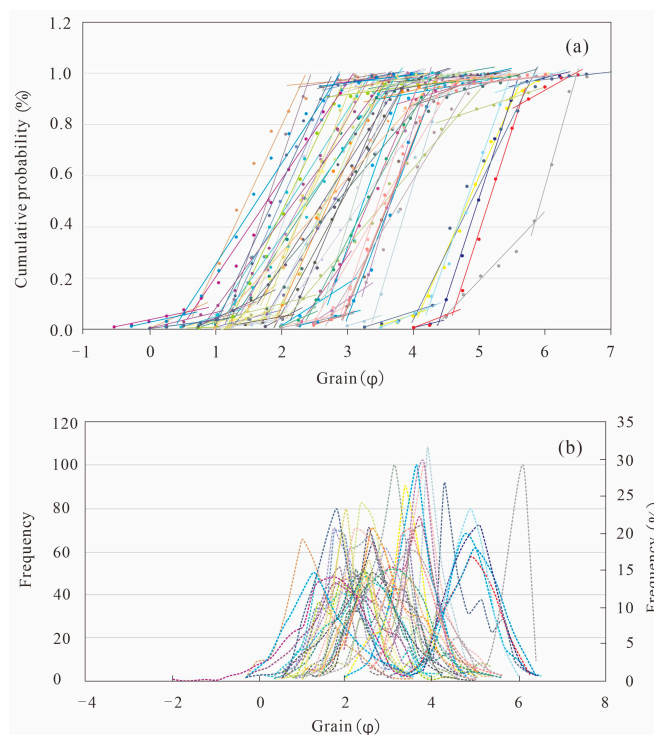


Figure 10. (a) Grain size distribution and (b) probability accumulation diagrams for sandstones of the Luohe Formation.

5. Discussion

5.1. Deposition Age

Radiometric age data for the Luohe Formation are lacking. A Middle–Late Ordovician age is inferred from graptolites, conodonts, and ostracods [67,68].

Detrital zircon ages can be used to determine the maximum depositional age of sedimentary rocks [69,70]. The youngest zircon grain of sample 20171013 from the Luohe Formation yields a U–Pb age of 451 ± 6 Ma; therefore, deposition must have occurred after 451 ± 6 Ma. In addition, the Luohe Formation strata are intruded by monzogranite that yields an age of 457.0 ± 6.5 Ma. Accordingly, deposition of the Luohe Formation occurred between 457.0 ± 6.5 and 451 ± 6 Ma; i.e., during the Late Ordovician.

5.2. Sedimentary Environment

The grain size in the lower part of the Luohe Formation is relatively coarse, and the rocks are mainly sandstones with minor mudstones that exhibit graded and parallel bedding. The grain size in the upper part of the Luohe Formation is relatively fine, and the rocks comprise mainly mudstones with minor sandstones that exhibit horizontal bedding. The rocks are compositionally immature and the grains are poorly rounded and well sorted. Cumulative probability curves for the samples exhibit a three-stage distribution, and frequency curves mainly show single peaks. Therefore, the lithological assemblage, sedimentary structures, and results of sedimentary grain-size analysis of the Luohe Formation are consistent with rapid, near-source deposition in a shallow marine environment.

5.3. Provenance

5.3.1. Detrital Zircon Geochronology

Zircon has a high closure temperature and high hardness, and its U–Pb isotopic system remains stable during various geological processes. Therefore, the detrital zircon age spectra from this study and geochronological data from the literature can be used to determine the sedimentary provenance [71].

Zircon age probability diagrams (Figure 7a,b) for sample 20171013 are characterized by predominant early Paleozoic age peaks at 504 and 463 Ma and subordinate Neoproterozoic peaks at 783, 826, and 973 Ma, with few grains having ages of >1.0 Ga. These data indicate that rocks in the source area are mainly Cambrian–Ordovician in age.

The predominant age peak is at 504 Ma. Most zircons have fine-scale oscillatory zoning with Th/U ratios of >0.1 , consistent with a magmatic origin. Therefore, these zircon grains were derived mainly from Cambrian magmatic rocks. Rocks with similar ages are well documented from the Erguna [72,73] and Xing'an [32] blocks in relation to magmatism that occurred in response to collision between the blocks [23,48].

The zircon grains with ages of ~ 463 Ma exhibit fine-scale oscillatory zoning and yield Th/U ratios of >0.1 , again indicating a magmatic origin. Therefore, these zircons were derived mainly from Ordovician magmatic rocks (Figure 7d–f). After the collision between the Erguna and Xing'an blocks, post-collisional magmatic intrusions were emplaced during 493–436 Ma [20,73–76]. The early Paleozoic Duobaoshan magmatic arc rocks were then emplaced in the southern margin of the Erguna–Xing'an Block during 485–467 Ma [39,41,49]. Therefore, zircons with an age of 463 Ma may have been derived from these two groups of magmatic rocks.

The subordinate Neoproterozoic peaks (783, 826, and 973 Ma) are mainly consistent with the ages of magmatic rocks in the northern–central Erguna Block (Figure 7c), including 929–737 Ma magmatic rocks in the Enhe and Mangui areas [76,77], 808 ± 2 Ma magmatic rocks in the Fenghuangshan area [78], and 915 ± 3 Ma gneissic granite in the Bowuleshan area [79].

Only eight zircons yield Mesoproterozoic or Mesoarchean ages, and these grains may have been derived from the ancient basement of the Erguna block (Figure 7c) including 1741–1854 Ma granitic gneiss and 1847 ± 4 Ma biotite plagioclase gneiss in the Hanjiayuanzi area [80], 2464 ± 26 Ma granitic gneiss in the Mohe area [81], and 2459–2562 Ma gneissic monzogranite in the southern Erguna mining area [82].

5.3.2. Sandstone Modal Analyses

The studied samples are medium- to coarse-grained sandstones. Grains are mainly subangular–subrounded and poorly to moderately sorted (Figure 7). Framework grains comprise mainly volcanic lithic fragments (20%–40%), quartz (25%–45%), and feldspar (15%–35%). The texture and composition of the sandstones are consistent with rapid deposition and a short transport distance. On ternary provenance discrimination diagrams [62], the samples plot mainly in the magmatic arc field, with some data in the recycled orogen field, indicating that the samples were not derived from a single source area, but that the main provenance area was a magmatic arc (Figure 11).

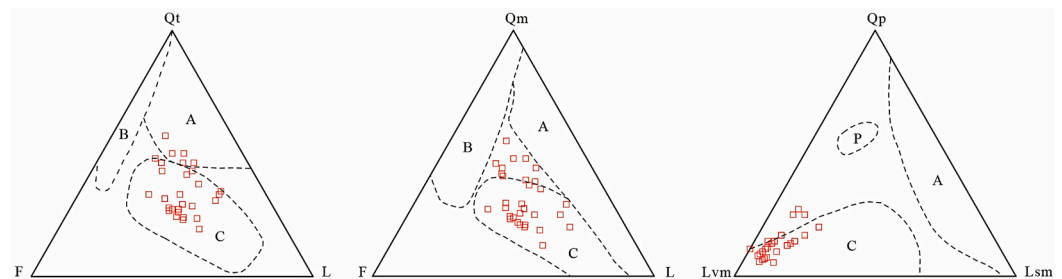


Figure 11. Ternary Qt–F–L, Qm–F–L, and Qp–Lvm–Lsm diagrams indicating the dynamic environment of sandstone from the Luohe Formation (after [62]). Qt—total quartz grains; Qp—polycrystalline quartz; Qm—monocrystalline quartz; F—total feldspar grains; Lvm—total volcanic–metavolcanic rock fragments; Lsm—total sedimentary–metasedimentary rock fragments. A—recycled orogenic belt; B—stable craton or uplifted basement; C—magmatic arc; P—accretionary wedge; □—the samples of sandstone modal analyses in this study.

5.3.3. Geochemistry Analyses

Values of $\text{SiO}_2/\text{Al}_2\text{O}_3$ can be used to infer the maturity of sedimentary rocks [83,84]. The $\text{SiO}_2/\text{Al}_2\text{O}_3$ values of sandstones from the Luohe Formation are 3.1–3.5, with an average of 3.4, indicating that the sandstones are of low maturity.

The REE patterns of sedimentary rocks reflect the properties of the source rocks [83–85]. The sandstones of the Luohe Formation are characterized by moderate enrichment in LREEs and relatively flat HREEs with a negative Eu anomaly (Figure 9a), indicating that the parent rocks were mainly felsic volcanic rocks. The Ba/Sr values of sandstones from the Luohe Formation are 2.03–5.02, with an average of 3.79, and the Rb/Sr values of sandstones from the Luohe Formation are 2.032–3.38, with an average of 2.72, the above two values are obviously higher than the values of the upper crust (2.55 and 0.32) [83], which indicates the source of the sandstones is the upper crust. In summary, the REE data indicate that the Luohe Formation was derived mainly from an upper crustal source.

Immobile element compositions in sandstones are closely related to the tectonic setting of deposition [86]. The contents and ratios of certain immobile elements can be used to identify four typical tectonic environments: oceanic island arc, continental island arc, active continental margin, and passive continental margin [84]. For the studied samples, most of the data plot in the continental island arc provenance field in a La–Th–Sc diagram (Figure 12).

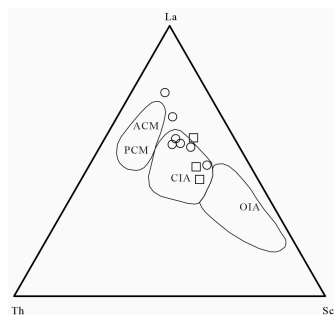


Figure 12. Ternary La–Th–Sc tectonic discrimination diagram for sandstones of the Luohe Formation. (□ from this study; ○ from [87]). ACM—active continental margin; PCM—passive continental margin; OIA—oceanic island arc; CIA—continental island arc.

5.4. Tectonic Implications

Based on geochronological and geochemical data, along with sandstone modal compositions, information on the sedimentary environment, and data from the literature, a new model is proposed for the Ordovician arc–basin system in the Northern Great Xing’an Range, Northeast China.

The collision between the Erguna and Xing’an blocks occurred before the late Cambrian, followed by the emplacement of late Cambrian granitic and mafic intrusions on either side of the Xinlin–Xiguitu suture zone [20,24,67]. During this period, the southern margin of the newly formed Erguna–Xing’an Block was a passive continental margin.

Subsequently, the Erguna–Xing’an Block transitioned to an epicontinental setting. During the Early Ordovician, an arc–basin system (i.e., the Duobaoshan island arc) formed in the southern margin of the Erguna–Xing’an Block in association with the subduction of the Paleo-Asian oceanic plate beneath the Erguna–Xing’an Block, and the Luohe Formation was deposited in the corresponding back-arc basin. Therefore, the Luohe Formation was derived mainly from magmatic rocks that were emplaced in response to the collision between the Erguna and Xing’an blocks, and the Duobaoshan island arc rocks formed in association with subduction of the Paleo-Asian oceanic plate. The ancient basement and Proterozoic granites of the Erguna block also provided a subordinate source for the Luohe Formation (Figure 13).

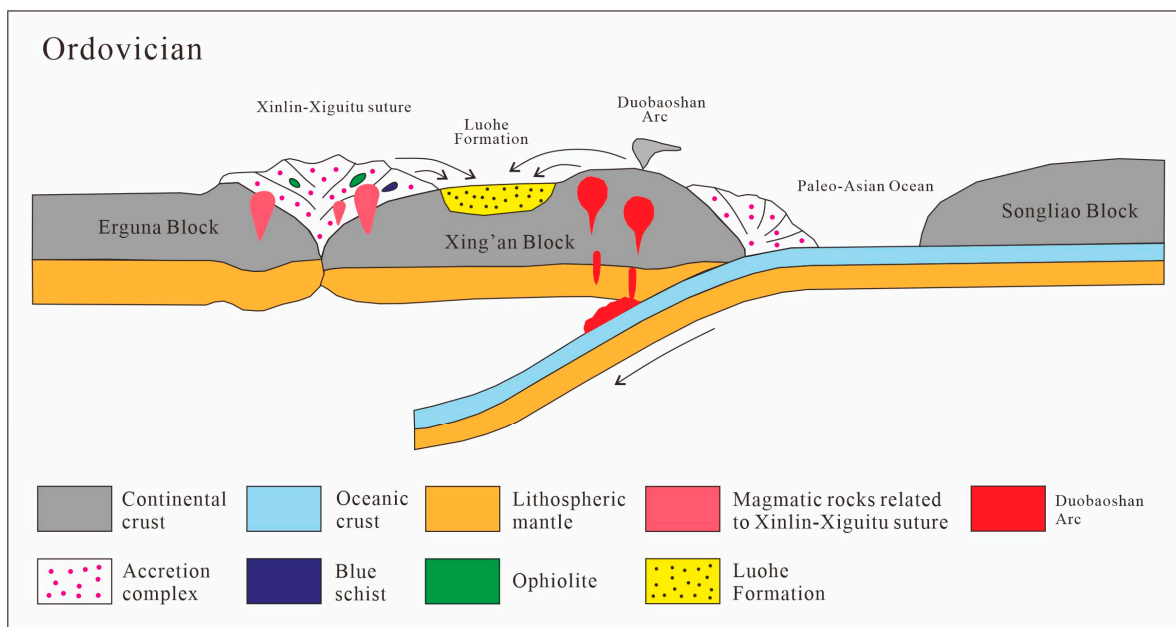


Figure 13. Schematic model of the Ordovician tectonic between the Songnen and Erguna–Xing’an blocks in the Wunuer area.

6. Conclusions

1. Based on the zircon age data of this study and the age of a monzogranite intrusion, the Luohe Formation was deposited between 457.0 ± 6.5 and 451 ± 6 Ma (i.e., Late Ordovician).
2. The detrital zircon age spectra for sandstones of the Luohe Formation show peak ages at 504 and 463 Ma, with subordinate Proterozoic and Neoproterozoic ages.
3. The zircon age distribution for the Luohe Formation rocks is consistent with the timing of periods of magmatism in the Erguna and Xing'an blocks. The youngest peak age of 463 Ma corresponds to the timing of post-collisional magmatism and the formation of the Duobaoshan island arc, and the second peak age of 504 Ma is consistent with magmatism that occurred in association with the collision between the Erguna and Xing'an blocks. The subordinate ages of 783, 826, 973, and 1882 Ma are consistent with magmatism in the Erguna block.
4. A new model of the tectonic evolution in the Northern Great Xing'an Range (Northeast China) during the Early Ordovician is proposed. Owing to the subduction of the Paleo-Asian oceanic lithosphere beneath the Erguna–Xing'an Block, an arc–basin system (i.e., the Duobaoshan island arc) was formed in the southern margin of the Erguna–Xing'an Block, and the Luohe Formation was deposited in the corresponding back-arc basin.

Supplementary Materials: The following supporting information can be downloaded at: <https://www.mdpi.com/article/10.3390/min14030258/s1>, Table S1: LA-ICP-MS U-Pb-Th data for zircons for sample 20171013. Table S2: Results of Sandstone modal analyses for Luohe Formation. Table S3: Statistics of granularity parameters of the Luohe Formation.

Author Contributions: Conceptualization, L.L. and Z.F.; methodology, L.L.; software, L.L.; validation, L.L., C.Z. and Z.F.; formal analysis, L.L.; investigation, L.L., C.Z. and Z.F.; resources, L.L. and Z.F.; data curation, L.L.; writing—original draft preparation, L.L.; writing—review and editing, L.L., C.Z. and Z.F.; visualization, L.L.; supervision, L.L., C.Z. and Z.F.; project administration, L.L. and Z.F.; funding acquisition, L.L. and C.Z. All authors have read and agreed to the published version of the manuscript.

Funding: This research was funded by the China Geological Survey Project (DD20230016, DD20221645, DD2016007808) and supported by the National Natural Science Foundation of China (Grant No. 42272251, 42072230 and 41602235).

Data Availability Statement: The original contributions presented in the study are included in the article/Supplementary Materials.

Acknowledgments: Special thanks are due to the reviewers and editors of this journal for their valuable suggestions and revisions of the manuscript.

Conflicts of Interest: The authors declare no conflict of interest.

References

1. Jahn, B.M.; Wu, F.Y.; Chen, B. Granitoids of the Central Asian Orogenic Belt and continental growth in the Phanerozoic. *Trans. R. Soc. Edinb.* **2000**, *91*, 181–194.
2. Jahn, B.M.; Wu, F.Y.; Chen, B. Massive granitoid generation in Central Asia: Nd isotope evidence and implication for continental growth in the Phanerozoic. *Episodes* **2000**, *23*, 82–92. [[CrossRef](#)] [[PubMed](#)]
3. Kröner, A.; Windley, B.F.; Badarch, G. Accretionary growth and crust-formation in the Central Asian Orogenic Belt and comparison with the Arabian–Nubian shield. *Geol. Soc. Am. Mem.* **2007**, *200*, 181–209.
4. Kröner, A.; Kovach, V.; Belousova, E.; Hegner, E.; Armstrong, R.; Dolgoplova, A.; Seltmann, R.; Alexeiev, D.V.; Hoffmann, J.E.; Wong, J. Reassessment of continental growth during the accretionary history of the Central Asian Orogenic Belt. *Gondwana Res.* **2014**, *25*, 103–125. [[CrossRef](#)]
5. Safonova, I.Y.; Sennikov, N.V.; Komiya, T. Geochemical diversity in oceanic basalts hosted by the Zasukh'ya accretionary complex, NW Russian Altai, Central Asia: Implications from trace elements and Nd isotopes. *J. Asian Earth Sci.* **2011**, *42*, 191–207. [[CrossRef](#)]
6. Safonova, I.; Maruyama, S. Asia: A frontier for a future supercontinent Amasia. *Int. Geol. Rev.* **2014**, *56*, 1051–1071. [[CrossRef](#)]
7. Yarmolyuk, V.V.; Kovach, V.P.; Kozakov, I.K. Mechanisms of continental crust formation in the Central Asian Foldbelt. *Geotectonics* **2012**, *46*, 251–272. [[CrossRef](#)]

8. Xiao, W.J.; Windley, B.F.; Hao, J.; Zhai, M.G. Accretion leading to collision and the Permian Solonker suture, Inner Mongolia, China: Termination of the central Asian orogenic belt. *Tectonic* **2003**, *22*, 1069. [[CrossRef](#)]
9. Xiao, W.J.; Santosh, M. The western Central Asian Orogenic Belt: A window to accretionary orogenesis and continental growth. *Gondwana Res.* **2014**, *25*, 1429–1444. [[CrossRef](#)]
10. Kovalenko, V.I.; Yarmolyuk, V.V.; Kovach, V.P.; Kotov, A.B.; Kozakov, I.K.; Salnikova, E.B.; Larin, A.M. Isotope provinces, mechanisms of generation and sources of the continental crust in the Central Asian mobile belt: Geological and isotopic evidence. *J. Asian Earth Sci.* **2004**, *23*, 605–627. [[CrossRef](#)]
11. Safonova, I.Y.; Santosh, M. Accretionary complexes in the Asia–Pacific region: Tracing archives of ocean plate stratigraphy and tracking mantle plumes. *Gondwana Res.* **2014**, *25*, 126–158. [[CrossRef](#)]
12. Dobretsov, N.L.; Berzin, N.A.; Buslov, M.M. Opening and tectonic evolution of the Paleo-Asian Ocean. *Int. Geol. Rev.* **1995**, *37*, 335–360. [[CrossRef](#)]
13. Windley, B.F.; Alexeiev, D.; Xiao, W.J.; Kröner, A.; Badarch, G. Tectonic models for accretion of the Central Asian Orogenic Belt. *J. Geol. Soc.* **2007**, *164*, 31–47. [[CrossRef](#)]
14. Safonova, I.; Kotlyarov, A.; Krivonogov, S.; Xiao, W.J. Intra-oceanic arcs of the PaleoAsian Ocean. *Gondwana Res.* **2017**, *50*, 167–194. [[CrossRef](#)]
15. Safonova, I.Y. Juvenile versus recycled crust in the Central Asian Orogenic Belt: Implications from ocean plate stratigraphy, blueschist belts and intraoceanic arcs. *Gondwana Res.* **2017**, *47*, 6–27. [[CrossRef](#)]
16. Li, J.Y. Permian geodynamic setting of Northeast China and adjacent regions: Closure of the Paleo-Asian Ocean and subduction of the Paleo-Pacific Plate. *J. Asian Earth Sci.* **2006**, *26*, 207–224. [[CrossRef](#)]
17. Kröner, A.; Lehmann, J.; Schulmann, K.; Demoux, A.; Lexa, O.; Tomurhuu, D.; Stipska, P.; Liu, D.; Wingate, M.T.D. Lithostratigraphic and geochronological constraints on the evolution of the Central Asian Orogenic Belt in SW Mongolia: Early Paleozoic rifting followed by late Paleozoic accretion. *Am. J. Sci.* **2010**, *310*, 523–574. [[CrossRef](#)]
18. Zheng, Y.F.; Xiao, W.J.; Zhao, G.C. Introduction to tectonic of China. *Gondwana Res.* **2013**, *23*, 1189–1206. [[CrossRef](#)]
19. Xiao, W.; Song, D.; Windley, B.F.; Li, J.; Han, C.; Wan, B.; Zhang, J.; Ao, S.; Zhang, Z. Accretionary processes and metallogenesis of the Central Asian Orogenic Belt: Advances and perspectives. *Sci. China Earth Sci.* **2020**, *63*, 329–361. [[CrossRef](#)]
20. Ge, W.C.; Wu, F.Y.; Zhou, C.Y.; Abdel Rahman, A.A. Emplacement age of the Tahe granite and its constraints on the tectonic nature of the Erguna block in the northern part of the Da Xing’an Range. *Chin. Sci. Bull.* **2005**, *50*, 2097–2105, (In Chinese with English Abstract).
21. Miao, L.C.; Fan, W.M.; Zhang, F.Q.; Liu, D.Y.; Jian, P.; Shi, G.H.; Tao, H.; Shi, Y.R. Zircon SHRIMP geochronology of the Xinkailing-Kele complex in the northwestern Lesser Xing’an Range, and its geological implications. *Chin. Sci. Bull.* **2004**, *49*, 201–209, (In Chinese with English Abstract). [[CrossRef](#)]
22. Miao, L.C.; Liu, D.Y.; Zhang, F.Q. Zircon SHRIMP U-Pb ages of the “Xinghuadukou Group” in Hanjiayuanzi and Xinlin areas and the “Zhalantun Group” in Inner Mongolia, Da Hinggan Mountains. *Chin. Sci. Bull.* **2007**, *52*, 1112–1134, (In Chinese with English Abstract). [[CrossRef](#)]
23. Miao, L.C.; Zhang, F.C.; Jiao, S.J. Age, protoliths and tectonic implications of the Toudaoqiao blueschist Inner Mongolia, China. *J. Asian Earth Sci.* **2015**, *105*, 360–373. [[CrossRef](#)]
24. Wu, F.Y.; Sun, D.Y.; Ge, W.C.; Zhang, Y.B.; Grant, M.L.; Wilde, S.A.; Jahn, B.M. Geochronology of the Phanerozoic granitoids in northeastern China. *J. Asian Earth Sci.* **2011**, *41*, 1–30. [[CrossRef](#)]
25. Xu, W.L.; Wang, F.; Pei, F.P.; Meng, E.; Tang, J.; Xu, M.J.; Wang, W. Mesozoic tectonic regimes and regional ore-forming background in NE China: Constraints from spatial and temporal variations of Mesozoic volcanic rock associations. *Acta Petrol. Sin.* **2013**, *29*, 339–353, (In Chinese with English Abstract).
26. Liu, Y.J.; Zhang, X.Z.; Jin, W.; Chi, X.G.; Wang, C.W.; Ma, Z.H.; Han, G.Q.; Wen, Q.B.; Li, W.; Wang, W.D.; et al. Late Paleozoic tectonic evolution in Northeast China. *Geol. China* **2010**, *37*, 943–951, (In Chinese with English Abstract).
27. Liu, Y.J.; Li, W.M.; Feng, Z.Q.; Wen, Q.B.; Neubauer, F.; Liang, C.Y. A review of the Paleozoic tectonics in the eastern part of Central Asian Orogenic Belt. *Gondwana Res.* **2017**, *43*, 123–148. [[CrossRef](#)]
28. Zhou, J.B.; Wilde, S.A.; Zhang, X.Z.; Zhao, G.C.; Liu, F.L.; Qiao, D.W.; Ren, S.M.; Liu, J.H. A N1300 km late Pan-African metamorphic belt in NE China: New evidence from the Xing’an block and its tectonic implications. *Tectonophysics* **2011**, *509*, 280–292. [[CrossRef](#)]
29. Zhou, J.B.; Wilde, S.A.; Zhang, X.Z.; Ren, S.M.; Zheng, C.Q. Early Paleozoic metamorphic rocks of the Erguna block in the Great Xing’an Range, NE China: Evidence for the timing of magmatic and metamorphic events and their tectonic implications. *Tectonophysics* **2011**, *499*, 105–117. [[CrossRef](#)]
30. Zhou, J.B.; Wang, B.; Wilde, S.A.; Zhao, G.C.; Cao, J.L.; Zheng, C.Q.; Zeng, W.S. Geochemistry and U-Pb zircon dating of the Toudaoqiao blueschists in the Great Xing’an Range, northeast China, and tectonic implications. *J. Asian Earth Sci.* **2015**, *97*, 197–210. [[CrossRef](#)]
31. Zhou, J.B.; Wilde, S.A. The crustal accretion history and tectonic evolution of the NE China segment of the Central Asian Orogenic Belt. *Gondwana Res.* **2013**, *23*, 1365–1377. [[CrossRef](#)]
32. Han, G.Q.; Liu, Y.J.; Neubauer, F.; Genser, J.; Li, W.; Zhao, Y.L.; Liang, C.Y. Origin of terranes in the eastern Central Asian Orogenic Belt, NE China: U-Pb ages of detrital zircons from Ordovician-Devonian sandstones, North Great Xing’an Range. *Tectonophysics* **2011**, *511*, 109–124. [[CrossRef](#)]

33. Han, G.Q.; Liu, Y.J.; Neubauer, F.; Genser, J.; Zhao, Y.L.; Wen, Q.B.; Li, W.; Wu, L.N.; Jiang, X.Y.; Zhao, L.M. Provenance analysis of Permian sandstones in the central and southern Da Xing'an Mountains, China: Constraints on the evolution of the eastern segment of the Central Asian Orogenic Belt. *Tectonophysics* **2012**, *580*, 100–113. [[CrossRef](#)]
34. Han, G.Q.; Liu, Y.J.; Neubauer, F.; Jin, W.; Genser, J.; Ren, S.M.; Li, W.; Wen, Q.B.; Zhao, Y.L.; Liang, C.Y. LA-ICP-MS U-Pb dating and Hf isotopic compositions of detrital zircons from the Permian sandstones in Da Xing'an Mountains, NE China: New evidence for the eastern extension of the Erenhot-Hegenshan suture zone. *J. Asian Earth Sci.* **2012**, *49*, 249–271. [[CrossRef](#)]
35. Han, G.Q.; Liu, Y.J.; Neubauer, F.; Bartel, E.; Genser, J.; Feng, Z.Q.; Zhang, L.; Yang, M.C. U-Pb age and Hf isotopic data of detrital zircons from the Devonian and Carboniferous sandstones in Yimin area, NE China: New evidences to the collision timing between the Xing'an and Erguna blocks in eastern segment of Central Asian Orogenic Belt. *J. Asian Earth Sci.* **2015**, *97*, 211–228. [[CrossRef](#)]
36. Xu, B.; Zhao, P.; Bao, Q.Z.; Zhou, Y.H.; Wang, Y.Y.; Luo, Z.W. Preliminary study on the pre-Mesozoic tectonic unit division of the Xing-Meng Orogenic Belt (XMOB). *Acta Petrologica Sinica* **2014**, *30*, 1841–1857, (In Chinese with English Abstract).
37. Xu, B.; Zhao, P.; Wang, Y.Y.; Liao, W.; Luo, Z.W.; Bao, Q.Z.; Zhou, Y.H. The pre-Devonian tectonic framework of Xing'an-Mongolia Orogenic belt (XMOB) in north China. *J. Asian Earth Sci.* **2015**, *97*, 183–196. [[CrossRef](#)]
38. Feng, Z.Q.; Liu, Y.J.; Liu, B.Q.; Wen, B.Q.; Li, W.M.; Liu, Q. Timing and nature of the Xinlin-Xiguitu Ocean: Constraints from ophiolitic gabbros in the northern Great Xing'an Range, eastern Central Asian Orogenic Belt. *Int. J. Earth Sci.* **2016**, *105*, 491–505. [[CrossRef](#)]
39. Wu, G.; Chen, Y.C.; Sun, F.Y.; Liu, J.; Wang, G.R.; Xu, B. Geochronology, geochemistry, and Sr-Nd-Hf isotopes of the early Paleozoic igneous rocks in the Duobaoshan area, NE China, and their geological significance. *J. Asian Earth Sci.* **2015**, *97*, 229–250. [[CrossRef](#)]
40. Liu, Y.J.; Feng, Z.Q.; Jiang, L.W.; Jin, W.; Li, W.M.; Guan, Q.B.; Wen, Q.B.; Liang, C.Y. Ophiolite in the eastern Central Asian Orogenic Belt, NE China. *Acta Petrol. Sin.* **2019**, *35*, 3017–3047, (In Chinese with English Abstract).
41. Liu, Y.J.; Li, W.M.; Ma, Y.F.; Feng, Z.Q.; Guan, Q.B.; Li, S.Z.; Chen, Z.X.; Liang, C.Y.; Wen, Q.B. An orocline in the eastern Central Asian Orogenic Belt. *Earth-Sci. Rev.* **2021**, *221*, 103808. [[CrossRef](#)]
42. Liu, Y.J.; Ma, Y.F.; Feng, Z.Q.; Li, W.M.; Li, S.Z.; Guan, Q.B.; Chen, Z.X.; Zhou, T.; Fang, Q.A. Paleozoic Orocline in the eastern Central Asian Orogenic Belt. *Acta Geol. Sin.* **2022**, *96*, 3468–3493, (In Chinese with English Abstract).
43. Ma, Y.F.; Liu, Y.J.; Peskov, A.Y.; Wang, Y.; Song, W.M.; Zhang, Y.J.; Qian, C.; Liu, T.J. Paleozoic tectonic evolution of the eastern Central Asian Orogenic Belt in NE China. *China Geol.* **2022**, *5*, 555–578. [[CrossRef](#)]
44. Li, J.Y.; Liu, J.F.; Qu, J.F.; Zheng, R.G.; Zhao, S.; Zhang, J.; Wang, L.J.; Zhang, X.W. Paleozoic tectonic units of Northeast China: Continental Blocks or Orogenic Belts? *Earth Sci.* **2019**, *44*, 3157–3177, (In Chinese with English Abstract).
45. Shao, J.A. *Crustal Evolution in the Middle Part of the Northern Margin of the Sino-Korean Plate*; Peking University Press: Beijing, China, 1991; pp. 1–136, (In Chinese with English Abstract).
46. Tang, K.D.; Shao, J.A.; Li, Y.F. Songnen massif and its research significance. *Earth Sci. Front.* **2011**, *18*, 57–65, (In Chinese with English Abstract).
47. Tong, Y.; Hong, D.W.; Wang, T.; Shi, X.J.; Zhang, J.J.; Zeng, T. Spatial and temporal distribution of granitoids in the middle segment of the Sino-Mongolian border and its tectonic and metallogenic implications. *Acta Geosci. Sin.* **2010**, *31*, 133–150, (In Chinese with English Abstract).
48. Feng, Z.Q.; Liu, Y.J.; Li, L.; Jin, W.; Jiang, L.W.; Li, W.M.; Zhao, Y.L. Geochemical and geochronological constraints on the tectonic setting of the Xinlin ophiolite, northern Great Xing'an Range, NE China. *Lithos* **2019**, *326*, 213–229. [[CrossRef](#)]
49. Zhao, C.; Qin, K.Z.; Song, G.X.; Li, G.M.; Li, Z.Z. Early Palaeozoic high-Mg basalt-andesite suite in the Duobaoshan Porphyry Cu deposit, NE China: Constraints on petrogenesis, mineralization, and tectonic setting. *Gondwana Res.* **2019**, *71*, 91–116. [[CrossRef](#)]
50. Chen, A.X.; Zhou, D.; Zhang, Q.K.; Guan, P.Y.; Yang, B. Tectonic and sedimentary environment in the Ordovician period of Central Xing'an Block. *Geoscience* **2016**, *30*, 1061–1071, (In Chinese with English Abstract).
51. Li, L.Y.; Liu, B. Sedimentary geological characteristics and sediment source of Luohe Formation in Wunuer Area, Great Xing'an Range. *Mod. Min.* **2020**, *617*, 37–45, (In Chinese with English Abstract).
52. Zhang, H.H.; Xu, D.B.; Zhang, K. Geochemical characteristic and sedimentary environment of the Devonian Niquihe Formation in northern Daxinganling Range. *Geol. Resour.* **2014**, *23*, 316–322, (In Chinese with English Abstract).
53. Zhang, Y.J.; Zhang, C.; Wu, X.W.; Cui, T.R.; Yang, Y.J.; Chen, H.J.; Jiang, B.; Guo, W.; Ma, Y.F. Geochronology and geochemistry of Late Paleozoic marine volcanic from the Zhalantun Area in Northern DaHinggan Mountains and its geological significance. *Acta Geol. Sin.* **2016**, *90*, 2706–2720, (In Chinese with English Abstract).
54. Zhao, Z.; Chi, X.G.; Liu, J.F.; Wang, T.F.; Hu, Z.C. Late Paleozoic arc-related magmatism in Yakeshi region, Inner Mongolia Chronological and geochemical evidence. *Acta Petrol. Sin.* **2010**, *26*, 3245–3258, (In Chinese with English Abstract).
55. Li, L.Y.; Chen, M.; Gong, Q.D.; Zhang, C.H.; Wang, X. Zircon U-Pb age, geochemical characteristics and geological significance of syenogranite in Wunuer area, Great Hinggan Mountains. *Geol. Rev.* **2019**, *65*, 389–400, (In Chinese with English Abstract).
56. Shao, J.D.; Tan, Q.; Wang, H.; Zhang, M.; He, H.Y. The Mesozoic strata and the Jurassic-Cretaceous boundary in the Daxinganling Region. *Geol. Resour.* **2011**, *20*, 4–11, (In Chinese with English Abstract).
57. Zhang, J.H.; Ge, W.C.; Wu, F.Y.; Wilde, S.A.; Yang, J.H.; Liu, X.H. Large-scale Early Cretaceous volcanic events in the northern Great Xing'an Range, northeastern China. *Lithos* **2008**, *102*, 138–157. [[CrossRef](#)]

58. Ludwig, K.R. *ISOPLLOT 3.00: A Geochronological Toolkit for Microsoft Excel*; Berkeley Geochronology Center: Berkeley, CA, USA, 2003.
59. Wiedenbeck, M.; Allé, P.; Corfu, F.; Griffin, W.; Meier, M.; Oberli, F.; Von Quadt, A.; Roddick, J.; Spiegel, W. Three natural zircon standards for U–Th–Pb, Lu–Hf, Trace element and REE analyses. *Geostand. Newslitt.* **1995**, *19*, 1–23. [[CrossRef](#)]
60. Wiedenbeck, M.; Hanchar, J.; Peck, W.; Sylvester, P. Further characterisation of the 91500 zircon crystal. *Geostand. Geoanal. Res.* **2004**, *28*, 9–39. [[CrossRef](#)]
61. Hou, K.J.; Li, Y.H.; Tian, Y.R. In situ U–Pb zircon dating using laser ablation–multi ion counting–ICP–MS. *Miner. Depos.* **2009**, *28*, 481–492, (In Chinese with English Abstract).
62. Dickinson, W.R. Interpreting provenance relations from detrital modes of sandstone. In *Provenance of Arenites*; Zuffa, G.G., Ed.; Reidel Publishing Co.: Dordrecht, The Netherlands, 1985; pp. 333–361.
63. Feng, Z.Q.; Liu, Y.J.; Li, W.M.; Zhao, Y.L.; Jiang, L.W. Detrital zircon U–Pb geochronology of the Ordovician sandstone and its constrain to the tectonic evolution of the northern Great Xing’an Range. *Acta Petrol. Sin.* **2021**, *35*, 1469–1488.
64. Jiang, L.W.; Liu, Y.J.; Feng, Z.Q.; Tang, C. Provenance and tectonic environment of Luohe Formation in northern Great Xing’an Range: Evidence from geochemistry and detrital zircon age. *Glob. Geol.* **2018**, *37*, 688–701.
65. Sahu, B.K. Depositional mechanisms from the size analysis of clastic sediment. *J. Sediment. Res.* **1964**, *34*, 2–24.
66. Mccave, I.N.; Syvitski, J.P.M. *Principles and Methods of Geological Particle Size Analysis*; Cambridge University Press: New York, NY, USA, 1991; pp. 3–21.
67. Yang, G.L.; He, Y.L.; Chen, J.L.; Wang, H.F.; Sun, B.N. The stratigraphic age and sedimentary environment of the Luohe Formation in the northeastern part of Inner Mongolia. In Proceedings of the Annual Meeting of Chinese Palaeontological Society, Dongyang, China, 1 November 2013; pp. 46–47, (In Chinese with English Abstract).
68. Ye, Q.; Yu, Y.; Gao, X.; Liu, S.F. Revision of the Ordovician Luohe Formation in Hanbeibudunzhao area of Altan Hil, Inner Mongolia. *Geol. Bull. China* **2013**, *32*, 1548–1557, (In Chinese with English Abstract).
69. Fedo, C.M.; Sircombe, K.N.; Rainbird, R.H. Detrital zircon analysis of the sedimentary record. *Rev. Mineral. Geochem.* **2003**, *53*, 277–303. [[CrossRef](#)]
70. Kalsbeek, F.; Frei, D.; Affaton, P. Constraints on provenance, stratigraphic correlation and structural context of the Volta basin, Ghana, from detrital zircon geochronology: An Amazonian connection? *Sediment. Geol.* **2008**, *212*, 86–95. [[CrossRef](#)]
71. Zhang, J.M.; Xu, B.; Yan, L.J.; Wang, Y.Y. Evolution of the Heihe–Nenjiang Ocean in the eastern Paleo-Asian Ocean: Constraints of sedimentological, geochronological and geochemical investigations from Early–Middle Paleozoic Heihe–Dashizhai Orogenic Belt in the northeast China. *Gondwana Res.* **2020**, *81*, 339–461. [[CrossRef](#)]
72. Wu, G.; Sun, F.Y.; Zhao, C.S.; Li, Z.T.; Zhao, A.L.; Pang, Q.B.; Li, G.Y. Discovery of the Early Paleozoic post-collisional granites in northern margin of the Erguna massif and its geological significance. *Chin. Sci. Bull.* **2005**, *50*, 2733–2743. [[CrossRef](#)]
73. Wu, G.; Chen, Y.; Chen, Y.; Zeng, Q. Zircon U–Pb ages of the metamorphic supracrustal rocks of the Xinghuadukou Group and granitic complexes in the Argun massif of the northern Great Hinggan Range, NE China, and their tectonic implications. *J. Asian Earth Sci.* **2012**, *49*, 214–233. [[CrossRef](#)]
74. Sorokin, A.A.; Kotov, A.B.; Sal’nikova, E.B.; Kudryashov, N.M.; Velikoslavinskii, S.D.; Yakovleva, S.Z.; Fedoseenko, A.M.; Plotkina, Y.V. Early Paleozoic Granitoids in the Lesser Khingan Terrane, Central Asian Foldbelt: Age, Geochemistry, and Geodynamic Interpretations. *Petrology* **2011**, *19*, 601–617. [[CrossRef](#)]
75. Ren, B.; Sun, L.; Cheng, Y.; Teng, X.; Li, Y.; Hao, S. Zircon U–Pb Ages, Hf isotopic Characteristics of the Yongqinglinchang–Shibazhan Granites in the Northern Da Hinggan Mountains, Northeastern China. *Geol. Surv. Res.* **2012**, *35*, 109–117, (In Chinese with English Abstract).
76. Gou, J.; Sun, D.Y.; Ren, Y.S.; Liu, Y.J.; Zhang, S.Y.; Fu, C.L.; Wang, T.H.; Wu, P.F.; Liu, X.M. Petrogenesis and geodynamic setting of Neoproterozoic and Late Paleozoic magmatism in the Manzhouli Erguna area of Inner Mongolia, China: Geochronological, geochemistry and Hf isotopic evidence. *J. Asian Earth Sci.* **2013**, *67–68*, 114–137. [[CrossRef](#)]
77. Tang, J.; Xu, W.L.; Wang, F.; Wang, W.; Xu, M.J.; Zhang, Y.H. Geochronology and geochemistry of Neoproterozoic magmatism in the Erguna Massif, NE China: Petrogenesis and implications for the breakup of the Rodinia supercontinent. *Precambrian Res.* **2013**, *224*, 597–611. [[CrossRef](#)]
78. Guo, Y.F.; Yang, Y.C.; Han, S.J.; Tan, Y.; Bo, J.W. Geochemistry and zircon U–Pb dating of the tonalite from Fenghuanshan area in northern Daxing’anling. *J. Jilin Univ. (Earth Sci. Ed.)* **2016**, *46*, 1406–1417, (In Chinese with English Abstract).
79. Yang, H.B.; Liu, Y.; Zheng, J.L.; Liang, Z.K.; Wang, X.Y.; Tang, X.F.; Sun, Y.P. Petrogenesis and geological significance of Neoproterozoic amphibolite and granite in Bowuleshan area, Erguna massif, Northeast China. *Geol. Bull. China* **2017**, *36*, 342–356, (In Chinese with English Abstract).
80. Sun, L.X.; Ren, B.F.; Zhao, F.Q.; Ji, S.P.; Geng, J.Z. Late Paleoproterozoic magmatic records in the Erguna Massif: Evidences from the zircon U–Pb dating of granitic gneisses. *Geol. Bull. China* **2013**, *32*, 341–352, (In Chinese with English Abstract).
81. Hou, W.; Zhao, G.; Han, Y.; Eizenhoefer, P.R.; Zhang, X.; Liu, Q. A ~2.5 Ga magmatic arc in NE China: New geochronological and geochemical evidence from the Xinghuadukou Complex. *Geol. J.* **2020**, *55*, 2550–2571. [[CrossRef](#)]
82. Shao, J.; Li, Y.F.; Zhou, Y.H.; Wang, H.B.; Zhang, J. Neo-Archaean magmatic event in Erguna Massif of Northeast China: Evidence from the zircon LA–ICP–MS dating of the gneissic monzogranite from the drill. *J. Jilin Univ. (Earth Sci. Ed.)* **2017**, *45*, 364–373, (In Chinese with English Abstract).

83. Taylor, S.R.; McLennan, S.M. *The Continental Crust: Its Composition and Evolution*; Blackwell Scientific Publications: Oxford, UK, 1985; p. 312.
84. McLennan, S.M.; Hemming, S.; McDaniel, D.K.; Hanson, G.N. Geochemical approaches to sedimentation, provenance and tectonics. In *Processes Controlling the Composition of Clastic Sediments*; Johnson, M.J., Basu, A., Eds.; Geological Society of America Special Paper 284; Geological Society of America: Boulder, CO, USA, 1993; pp. 21–40.
85. McLennan, S.M.; Hemming, S.; Taylor, S.R.; Eriksson, K.A. Early Proterozoic crustal evolution: Geochemical and Nd-Pb isotopic evidence from metasedimentary rocks, southwestern North America. *Geochem. Cosmochim. Acta* **1995**, *59*, 1153–1177. [[CrossRef](#)]
86. Bhatia, M.R.; Crook, K.A.W. Trace element characteristics of graywackes and tectonic setting discrimination of sedimentary basins. *Contrib. Mineral. Petrol.* **1986**, *92*, 181–193. [[CrossRef](#)]
87. Xiao, X.; Wang, S.H.; Liu, Z.H.; Mai, M.T.; Zeng, Z. Geochemistry characteristics and provenance of the Ordovician Luohe Formation clastic rocks in the northern Great Xing'an Range. *West-China Explor. Eng.* **2016**, *28*, 138–142. (In Chinese)

Disclaimer/Publisher's Note: The statements, opinions and data contained in all publications are solely those of the individual author(s) and contributor(s) and not of MDPI and/or the editor(s). MDPI and/or the editor(s) disclaim responsibility for any injury to people or property resulting from any ideas, methods, instructions or products referred to in the content.